IEEE Access
Multidisciplinary | Rapid Review | Open Access Journal

Received September 19, 2019, accepted September 26, 2019, date of publication October 3, 2019, date of current version October 16, 2019.

Digital Object Identifier 10.1109/ACCESS.2019.2945369

Complex Singular Spectrum Decomposition and Its Application to Rotating Machinery Fault Diagnosis

BIN PANG, GUIJI TANG, AND TIAN TIAN
Department of Mechanical Engineering, North China Electric Power University, Baoding 071003, China
Corresponding author: Guiji Tang (tanggjlk@ncepu.edu.cn)

This work was supported in part by the National Natural Science Foundation of China under Grant 51777074, in part by the Fundamental Research Funds for the Central Universities under Grant 2017XS134, and in part by the Top Youth Talent Support Program of Hebei Province under Grant [2018]-27.

ABSTRACT In recent years, singular spectrum decomposition (SSD) has been recognized as a powerful signal decomposition technique and has become a useful tool for fault signature extraction of rotating machinery. A complex SSD (CSSD) approach is proposed in this paper, extending SSD to the complex domain. Moreover, the equivalent filter banks property of CSSD is studied by using the Gaussian noise. Based on the CSSD and Hilbert transform (HT), two fault feature extraction algorithms, named CSSD Hilbert time-frequency spectrum (CSSD-HTFS) and CSSD Hilbert envelope spectrum (CSSD-HES), are exploited. In order to fuse the information of multi-sensors and extract sufficient fault features, a novel fault diagnosis framework for rotating machinery is developed. Specifically, the vibration signals collected along the X-direction and Y-direction are firstly employed to construct a complex-valued signal. Next, the CSSD of the complex-valued signal is carried out to obtain a series of decomposed components associated with the positive and negative frequency components. Following, the CSSD-HTFS or the CSSD-HES algorithm is adopted to extract the fault signatures of the decomposed components. Finally, the fault pattern of the rotating machinery is recognized based on the extracted fault signatures. Several examples of fault diagnosis applications validate the developed methodology.

INDEX TERMS Complex singular spectrum decomposition, complex-valued signal analysis, homologous information fusion, rotating machinery, fault diagnosis.

NOMENCLATURE

SSD	Singular spectrum decomposition
CSSD	Complex singular spectrum decomposition
HT	Hilbert transform
CSSD-HTFS	Complex singular spectrum decomposition-Hilbert time-frequency spectrum
HES	Hilbert envelope spectrum
CSSD-HES	Complex singular spectrum decomposition-Hilbert envelope spectrum
REB	Rolling element bearing
EMD	Empirical mode decomposition
LMD	Local mean decomposition
LCD	Local characteristic scale decomposition
VMD	Variational mode decomposition
ASTFA	Adaptive sparsest time-frequency analysis
SWD	Swarm decomposition
SSA	Singular spectrum analysis
BEMD	Bivariate empirical mode decomposition
CEMD	Complex empirical mode decomposition
CLMD	Complex local mean decomposition
CVMD	Complex variational mode decomposition
CSSA	Complex singular spectrum analysis
SVD	Singular value decomposition
SSC	Singular spectrum component
TFA	Time-frequency analysis
HHT	Hilbert-Huang transform
IA	Instantaneous amplitude
IF	Instantaneous frequency
CSSC	Complex singular spectrum component

The associate editor coordinating the review of this manuscript and approving it for publication was Li He.

I. INTRODUCTION

Rotating machinery is one of the most widely used machinery types in industrial production [1]. The typical machinery components, such as rolling element bearing (REB), gear and rotor, are high fault rate mechanical components, and their failures may cause pecuniary losses and even casualties [2]. Thus, fault diagnosis of these critical rotating machinery components is of the highest importance in the academic research and engineering applications [3].

The fault types of rotating machinery are abundant. For example, common faults of the rotor mainly include unbalance, rubbing, oil film instability and rotor cracks. The major failure modes of REB and gear are local damages, such as pitting, fracture, spalling and wear. Previous studies have concluded that the vibration signal of each specific rotating machinery fault has a corresponding fault signature. Generally, the rotor fault vibration signal is composed of several harmonic components related to the fundamental frequency signal. The fault vibration signals of the REB and gear are mainly characterized by the periodic impact characteristic. Vibration monitoring and analysis have become two significant aspects of rotating machinery fault diagnosis [4]. A critical step in rotating machinery fault diagnosis based on vibration analysis is the application of advanced signal processing tools, such as spectral kurtosis [5], deconvolution [6], and signal decomposition [7], to retrieve fault features from the vibration data. Among these signal processing tools, signal decomposition plays the most crucial role in fault signature extraction owning to its advantages in excluding the interferences and remaining the useful information. Current signal decomposition methods can be divided into different types based on their principles. Some of them can be summarized as wavelet transform and wavelet packet transform methods based on various forms of basis functions. Such methods require a pre-set basis function that matches the waveform of the fault signal, making them less adaptive [8]. Some signal decomposition algorithms are developed with reference to the morphological features of the signal. Among them, empirical mode decomposition (EMD) as a recursive decomposition approach is the most primitive and representative [9]. Inspired by EMD, other recursive decomposition approaches, e.g., local mean decomposition (LMD) [10] and local characteristic scale decomposition (LCD) [11], have been later proposed. This class of decomposition methods has good adaptability, so it can be characterized as genuinely data-driven. However, they have no appropriate mathematical models and are susceptible to mode mixing [12]. In recent years, some innovative signal decomposition approaches, such as variational mode decomposition (VMD) [13], adaptive sparsest time-frequency analysis (ASTFA) [14] and swarm decomposition (SWD) [15], have been exploited. These methods can be characterized as parameterized model methods, while their parameters selection process usually hinders their online applications. Singular spectrum analysis (SSA) is another prominent signal decomposition approach, which has been used in various fields owing to its excellent merits in dealing with non-stationary signals [16]. In the decomposition framework of SSA, the embedding dimension is required to be pre-set, while the principal components need to be grouped reasonably. How to implement the adaptive setting of these two parameters is a problem of SSA.

Singular spectrum decomposition (SSD) was exploited by Bonizzi *et al.* [17] to solve the aforementioned issues of SSA. SSD keeps all good merits of SSA and performs very well in non-stationary signal decomposition. Considering the advantages of SSD, many researchers have successfully introduced the original SSD or developed modified SSD methods to diagnose the faults of REB [18] and gear [19], [20]. However, the SSD method can only analyze the real-valued signals and can only deal with the vibration signal of a single sensor. In recent years, the complex-valued signal analysis has flourished in various research fields. Scholars have contributed to extending the real-valued decomposition methods to the complex domain. The SSA method can be directly applied to the complex-valued signals to perform the complex SSA (CSSA) analysis [21], [22]. Complex-valued Hankel is used in the CSSA method, placing a huge computational burden on the process. In addition, CSSA relies on experience to implement the setting of embedding dimension and the grouping of principal components. Rilling *et al.* invented the bivariate EMD (BEMD) method to process the bivariate signals [23]. BEMD is the extended application of EMD into the complex domain. BEMD demonstrated great performance in the wind turbine condition monitoring [24]. Inspired by BEMD, Park *et al.* developed a complex LMD (CLMD) approach [25]. However, both BEMD and CLMD are only suitable for the signals connected in Cartesian coordinates [23]. Another complex signal decomposition algorithm, called complex EMD (CEMD) [26], was invented by conducting EMD on the real and imaginary frequency components of the complex signal, respectively. Compared to BEMD, CEMD is adaptive to a wider range of conditions. In addition, it has shown advantages in information fusion. Motivated by the CEMD algorithm, a complex VMD (CVMD) method was developed [27]. CVMD demonstrates a stronger decomposition capability compared to CEMD. However, the tedious parameter selection problem inherited from VMD remains a serious flaw of CVMD. Motivated by the works of CEMD and CVMD, a complex SSD (CSSD) algorithm is developed to enable SSD to process the complex-valued signals. CSSD is more adaptive than CSSA as it is an approach independent of parameters selection. After the signal decomposition, the extraction of the characteristic information from the decomposed components is of critical importance. Time-frequency analysis (TFA) and demodulation analysis are two powerful tools for fault features extraction. Specifically, TFA has been widely used for rotor fault diagnosis as it can detect the signal frequency composition. Demodulation analysis is indispensable

in identifying the fault characteristic frequencies of REB and gear. In this paper, the proposed CSSD algorithm is combined with the Hilbert transform (HT) to perform the CSSD Hilbert time-frequency spectrum (CSSD-HTFS) and CSSD Hilbert envelope spectrum (CSSD-HES) analysis. The CSSD-HTFS is used for rotor fault feature extraction, while the CSSD-HES is adopted to extract the fault characteristic frequencies of REB and gear.

The inherent dynamic characteristics of rotating machinery in fault state are very complicated, while the features of the vibration signals in different directions may vary significantly. Diagnosing the type of failure of a rotating machine through the fault characteristics of a single-channel signal is prone to false judgment. Thus, scholars have focused their research on condition monitoring techniques based on multi-sensors. Among them, a simple and effective way has proven to be the arrangement of sensors to collect vibration information in two perpendicular directions [28]. However, the fusion of homologous information proves difficult. In this work, a novel fault diagnosis framework based on CSSD is developed to detect the synchronous information in multi-channel signals, while its validity is investigated by using experimental fault signals.

The structure of this paper is as follows. The SSD algorithm is briefly recalled in Section II. Section III presents the CSSD algorithm and studies the filter bank property of CSSD, while the CSSD-HTFS and CSSD-HES analysis methods are also introduced in this part. Section IV addresses the fault diagnosis framework based on CSSD. Section V examines the effectiveness of the fault diagnosis framework through several applications. The conclusion is presented in Section VI.

II. SINGULAR SPECTRUM DECOMPOSITION

SSD is an iterative signal decomposition method, which can adaptively extract the component signals of a composite signal. Its development aims to promote the adaptability of the SSA algorithm. Specifically, the auto-generated selection of the embedding dimension for the trajectory matrix construction, as well as the adaptive grouping of the singular value decomposition (SVD) components for the reconstruction of a specific sub-series are achieved. The decomposition series of SSD is named singular spectrum component (SSC). Given a composite signal $s(n)$ of length N, the main steps of SSD at each iteration include:

(1) Embedding

The first step of the SSD algorithm is to choose the embedding dimension to build the trajectory matrix. For an original composite signal $s(n)$, the trajectory matrix corresponding to the embedding dimension M is:

$$\mathbf{S} = [\mathbf{s}_1^{\mathrm{T}}, \mathbf{s}_2^{\mathrm{T}}, \cdots, \mathbf{s}_M^{\mathrm{T}}]^{\mathrm{T}} \tag{1}$$

where $\mathbf{s}_j = (s(j), \ldots, s(N), s(1), \ldots, s(j-1))$ $(j = 1 \ldots, M)$ denotes the j-th row of the trajectory matrix.

The trajectory matrix shown in Equation (1) is composed of N column vectors, while the first $N-M+1$ ones establish the trajectory matrix employed in the primitive SSA algorithm. The modified definition of the trajectory matrix in the SSD algorithm can contribute to boosting the oscillating elements of the signal.

From Equation (1), it is derived that the value of the embedding dimension determines the expression of the trajectory matrix. So, the choice of this parameter can affect the final results distinctively. A shortcoming of the primitive SSA method is that the optimal embedding dimension at each iteration cannot be determined adaptively. This issue is solved in the SSD algorithm according to the following criterion:

(a) At iteration j, the residual signal is expressed as: $r_j(n) = s(n) - \sum_{k=1}^{j-1} r_k(n) (r_0(n) = s(n))$. The chief frequency $f_{\max}$ corresponding to the highest amplitude in the power spectral density (PSD) of $r_j(n)$ should first be detected.

(b) For $j = 1$, the remaining component is characterized as a significant trend in the case of $f_{\max}/F_s < 10^{-3}$ (F_s is the sampling frequency), while M is considered as $N/3$.

(c) Otherwise, and for $j > 1$, M is selected as $1.2\, F_s/f_{max}$.

(2) SVD

The trajectory matrix $\mathbf{S}$ reflects the global information of the current residual signal. Thus, it is subjected to SVD to detect its inherent components:

$$\begin{aligned}
\mathbf{S} &= \mathbf{A}\mathbf{U}\mathbf{B}^{\mathrm{T}} \\
&= [\mathbf{a}_1, \mathbf{a}_2, \cdots, \mathbf{a}_M] \begin{bmatrix} u_1 & 0 & 0 & 0 & 0 \\ 0 & u_2 & 0 & 0 & 0 \\ \vdots & \vdots & \ddots & \vdots & 0 \\ 0 & 0 & 0 & u_M & 0 \end{bmatrix} \begin{bmatrix} \mathbf{b}_1^{\mathrm{T}} \\ \mathbf{b}_2^{\mathrm{T}} \\ \vdots \\ \mathbf{b}_N^{\mathrm{T}} \end{bmatrix} \\
&= u_1 \mathbf{a}_1 \mathbf{b}_1^{\mathrm{T}} + u_2 \mathbf{a}_2 b_2^{\mathrm{T}} + \cdots + u_M \mathbf{a}_M \mathbf{b}_M^{\mathrm{T}} \\
&= \mathbf{S}_1 + \mathbf{S}_2 + \cdots + \mathbf{S}_M
\end{aligned} \tag{2}$$

where $\mathbf{A} \in \mathbf{R}^{M \times M}$, $\mathbf{U} \in \mathbf{R}^{M \times N}$, $\mathbf{B} = \mathbf{R}^{N \times N}$, $\mathbf{S}_i = u_i \mathbf{a}_i \mathbf{b}_i$ $(i = 1, \ldots, M)$ is the i-th SVD component of the trajectory matrix.

(3) Selection of the SVD components and extraction of the$j$-th component signal

Based on the SVD analysis, M component matrices (i.e., the SVD components) of the trajectory matrix are retrieved. However, only several of these SVD components are useful for the extraction of the j-th component signal $\mathrm{SSC}_j(n)$. Following, the solution adopted by SSD is described.

(a) During the first iteration, if a significant trend is evident, only the SVD component $\mathbf{S}_1$ is helpful, while the first component $\mathrm{SSC}_1(n)$ is extracted from the diagonal average of $\mathbf{S}_1$.

(b) For $j > 1$, the frequency contents of the component signal SSC_j are concentrated in the frequency band $[f_{max} - f_d, f_{max} + f_d]$, where f_d denotes the primary peak width of the PSD of $r_j(n)$. Thus, a subclass K_j ($K_j = \{k_1, \ldots, k_l\}$) is established, where k_j represents the order number of the SVD component S_{k_j}, whose left eigenvector displays a principal frequency in $[f_{max} - f_d, f_{max} + f_d]$. Finally, the reconstruction of $\mathrm{SSC}_j(n)$ is completed with the diagonal averaging calculation of the matrix $\mathbf{S}_{K_j} = \mathbf{S}_{k_1} + \cdots \mathbf{S}_{k_l}$.

(4) Stopping criterion

A new residual can be generated after the separation of the estimated component $SSC_j(n)$ from the current residual:

$$r_{j+1}(n) = r_j(n) - SSC_j(n) \tag{3}$$

$r_j(n)$ will be used as the input to perform the next decomposition. If the formula in Eq. (4) is less than a pre-set threshold, the decomposition should be terminated.

$$E_j = \sum_{k=1}^{N} (r_{j+1}(k))^2 \Big/ \sum_{k=1}^{N} (s(k))^2 \tag{4}$$

III. COMPLEX SINGULAR SPECTRUM DECOMPOSITION

A. CSSD ALGORITHM

Inspired by the CEMD method, a CSSD algorithm is developed to extend the SSD analysis to the complex domain. Given a complex signal $s(n)$, its Fourier transform spectrum $S(e^{j\omega})$ is bidirectional, composed of the positive and negative frequency parts. Two analytical signals related to these two parts can be generated as:

$$S_+(e^{j\omega}) = H(e^{j\omega})S(e^{j\omega}) \tag{5}$$
$$S_-(e^{j\omega}) = H(e^{j\omega})S^*(e^{-j\omega}) \tag{6}$$

where $S^*(e^{j\omega})$ denotes the complex conjugate of $S(e^{j\omega})$, and $H(e^{j\omega})$ represents a band-pass filter described as:

$$H(e^{j\omega}) = \begin{cases} 1, & 0 \le \omega < \pi \\ 0, & -\pi \le \omega < 0 \end{cases} \tag{7}$$

Two real signals associated with the positive and negative frequencies can be further described as:

$$s_+(n) = \Re\{F^{-1}(S_+(e^{j\omega})\} \tag{8}$$
$$s_-(n) = \Re\{F^{-1}(S_-(e^{j\omega})\} \tag{9}$$

where $\Re[\cdot]$ is the operator, which can be used for extracting the real parts of the complex signals, while $F^{-1}[\cdot]$ represents the inverse Fourier transform.

Owing to the good merits of the analytical signals, the original complex signal can be reconstructed by employing Equation (10):

$$s(n) = (s_+(n) + jh[s_+(n)]) + (s_-(n) + jh[s_-(n)])^* \tag{10}$$

where $h[\cdot]$ denotes the HT operator.

The two real signals $s_+(n)$ and $s_-(n)$ contain all the information of the original complex signal. Next, SSD is applied to $s_+(n)$ and $s_-(n)$ separately to conduct the CSSD analysis as follows:

$$s_+(n) = \sum_{i=1}^{N} s_i(n) \tag{11}$$

$$s_-(n) = \sum_{i=-N}^{-1} s_i(n) \tag{12}$$

where $\{s_i(n)\}_{i=1}^{N}$ and $\{s_i(n)\}_{i=-N}^{-1}$ represent groups of SSCs corresponding to $s_+(n)$ and $s_-(n)$, respectively.

We can deduce the final expression of the proposed CSSD for a complex-valued signal based on Equations (10)-(12):

$$s(n) = \sum_{i=-N, i\neq 0}^{N} z_i(n) \tag{13}$$

where $z_i(n)$ represents the i-th complex SSC (CSSC), which is defined as:

$$z_i(n) = \begin{cases} s_i(n) + jy_i(n), & i = 1, \ldots, N \\ (s_i(n) + jy_i(n)^*, & i = -N, \ldots, -1 \end{cases} \tag{14}$$

where $y_i(n) = h[s_i(n)]$.

A complex signal $s(t)$ as expressed in Equation (15) is employed to illustrate the reasoning of the method used in CSSD to separate the information of the original complex signal into two sub-components $s_+(t)$ and $s_-(t)$. Note that the sampling frequency of the complex signal is 1024 Hz.

$$s(t) = 0.5\sin(2\pi 40t) + j\cos(2\pi 60t), \quad t \in [0, 0.5] \tag{15}$$

Based on Equations (8) and (9), two real signals, i.e., $s_+(t)$ and $s_-(t)$, are firstly obtained as illustrated in Fig. 1(a) and (b), respectively. Then, a complex signal can be recovered by using Equation (10). The real and imaginary parts of the recovered complex signal are separately depicted in Fig. 1(c) and (d) (refer to the red lines). The real and imaginary parts of $s(t)$ are also represented in Fig. 1(c) and (d) (represented by the blue lines). The real and imaginary parts of the recovered signal exhibit similar waveforms to that of the original signal. Note that the slight phase shift between the original and the recovered signals appears as the signal reconstruction process involves the HT operator, which does not affect the result. Fig. 2 illustrates the frequency spectrums of the recovered and original signals. It is evident the two spectrums are very consistent, which further illustrates the feasibility of the CSSD algorithm.

B. CSSD EQUIVALENT FILTER BANKS

Motivated by the work in [26] and [29], the filter bank property of the CSSD method is studied in this section. First, a set of 1500 independent Gaussian complex-valued time sequences of 1024 samples were randomly generated. The CSSD algorithm with a preset mode number of four was then applied to the complex-valued time sequences, while the power spectra of the decomposed CSSCs were averaged. Fig. 3 displays the results corresponding to the first four CSSCs. The decomposed CSSCs show different frequency-bands. The CSSD decomposition is equal to the filter bank analysis. This result demonstrates the validity of the CSSD algorithm for detecting the sub-band components with different frequency-bands.

C. CSSD HILBERT TIME-FREQUENCY SPECTRUM

TFA is a prevailing tool for processing multi-component non-stationary signals. A simple framework to realize the

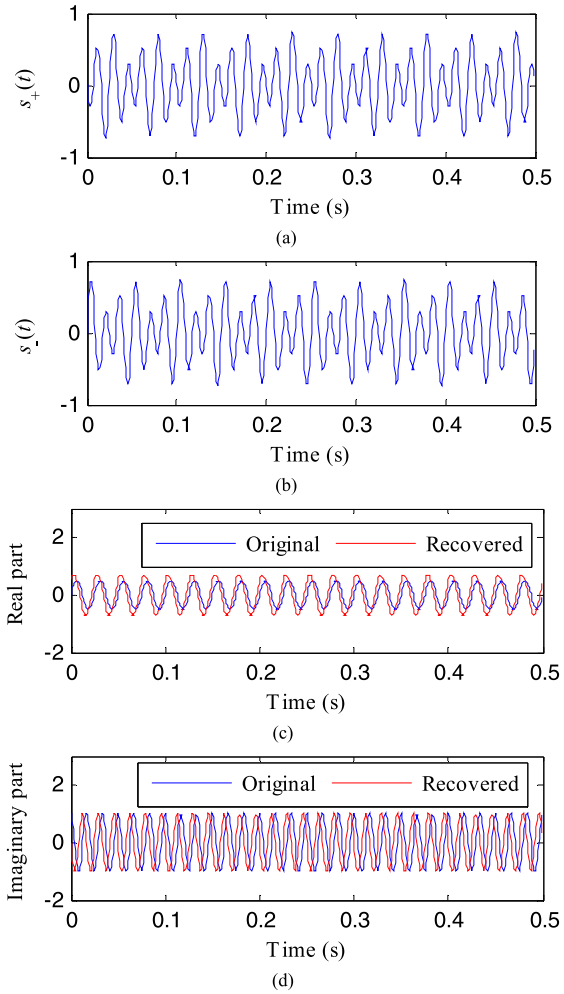

FIGURE 1. (a) $s_+(t)$; (b) $s_-(t)$; (c) the real part of the original and recovered signals; (d) the imaginary part of the original and recovered signals.

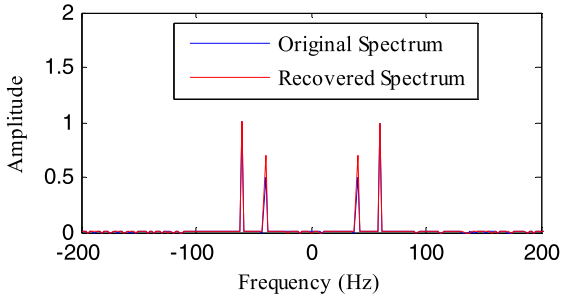

FIGURE 2. The frequency spectrums of the original and recovered signals.

TFA for real-valued signals is to combine signal decomposition algorithms with demodulation techniques. Hilbert-Huang transform (HHT) is an excellent example of this class of TFA methods. HHT is realized by using HT to compute the instantaneous amplitude (IA) and the instantaneous frequency (IF) of each decomposition series of EMD. Wang *et al.* [27] pioneered a TFA approach for complex-valued signals by integrating CVMD and HT. Motivated by the work of [27], a CSSD Hilbert time-frequency

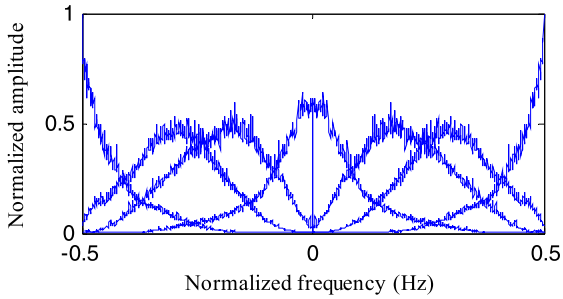

FIGURE 3. CSSD equivalent filter banks.

spectrum (CSSD-HTFS) method is proposed, which aims to extract the time-frequency information of complex-valued signals. Based on Equation (14), we can deduce that the complex SSCs of the positive and negative frequency components of a continuous-time complex-valued signal $s(t)$ can be represented using the analytic signal [27]:

$$z_i(t) = \begin{cases} a_i(t)e^{j\varphi_i(t)}, & i = 1, \ldots, N \\ a_i(t)e^{-j\varphi_i(t)}, & i = -N, \ldots, -1 \end{cases} \tag{16}$$

in which $a_i(t) = \sqrt{s_i(t)^2 + y_i(t)^2}$ is the IA, and $\varphi_i(t) = \arctan(y_i(t)/s_i(t))$ represents the instantaneous phase (IP). The IF can be further deduced as;

$$f_i(t) = \frac{\mathrm{sgn}(i)}{2\pi}\frac{df_i(t)}{dt}, \quad i = -N, \ldots, -1, 1, \ldots, N \tag{17}$$

Thus, the CSSD-HTFS for a continuous-time complex-valued signal can be represented as:

$$s(t) = \sum_{i=-N, i\neq 0}^{N} a_i(t)e^{j\int 2\pi f_i(t)dt} \tag{18}$$

D. CSSD HILBERT ENVELOPE SPECTRUM

The vibration signal of many rotating machinery faults has prominent modulation characteristics. Hence, demodulation analysis is a crucial tool in fault signature extraction. Among the reported demodulation methods, Hilbert envelope spectrum (HES) is the most notable. HES is defined as the Fourier transform spectrum of the envelope signal, i.e., the IA signal as introduced above. In this work, CSSD is combined with HES to perform the CSSD-HES demodulation analysis of a complex-valued signal. As the amplitude of the HES of the decomposed sequences of the positive and negative frequency components exhibit significant differences, the HES analysis of the decomposition sequences is conducted separately. Fig. 4 illustrates the flowchart of the CSSD-HES analysis for a complex-valued signal.

IV. FAULT DIAGNOSIS FRAMEWORK BASED ON CSSD

The rotating machinery usually has a complex structure. The vibration signals in different directions exhibit different characteristics. Hence, multi-sensors are usually arranged along various directions to obtain as much useful information as possible during the condition monitoring of rotating machinery. In order to fuse the information collected from

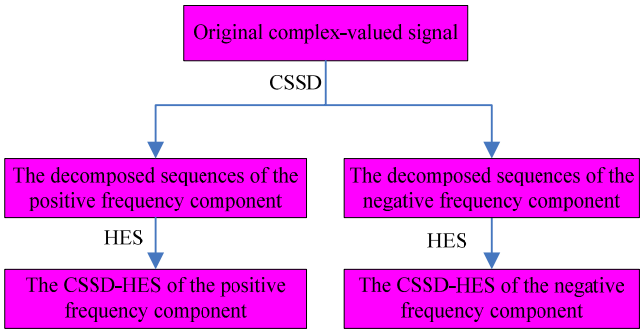

FIGURE 4. Flowchart of the CSSD-HES analysis.

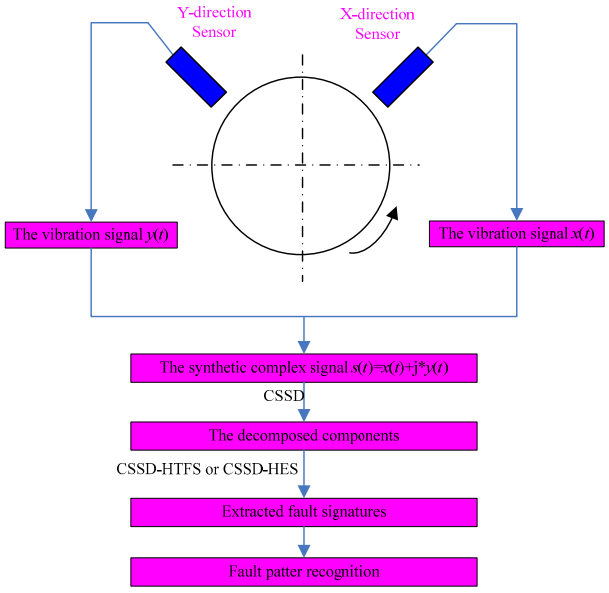

FIGURE 5. The fault diagnosis framework based on CSSD.

the multi-sensors to extract sufficient fault signatures, a novel fault diagnosis framework as depicted in Fig. 5 is developed based on the good merits of CSSD. This can be described as follows:

(1) Locate two sensors in the X-direction and Y-direction to collect the homologous vibration signals $x(t)$ and $y(t)$.

(2) Synthesize a complex signal: $s(t) = x(t) + \mathrm{j} * y(t)$.

(3) Apply CSSD to the synthetic complex signal to obtain the decomposed components.

(4) Detect the fault signatures of the CSSD decompositions by employing the CSSD-HTFS or the CSSD-HES algorithm.

(5) Recognize the fault pattern based on the detected fault signatures.

V. APPLICATIONS

A. ANALYSIS OF ROTOR RUBBING FAULT SIGNAL

The proposed CSSD approach is adopted to analyze the local rubbing fault signal to highlight its validity. Fig. 6(a) shows the test rig employed to simulate the rotor rubbing fault. The test rig is driven by a DC motor. A shaft, carrying a

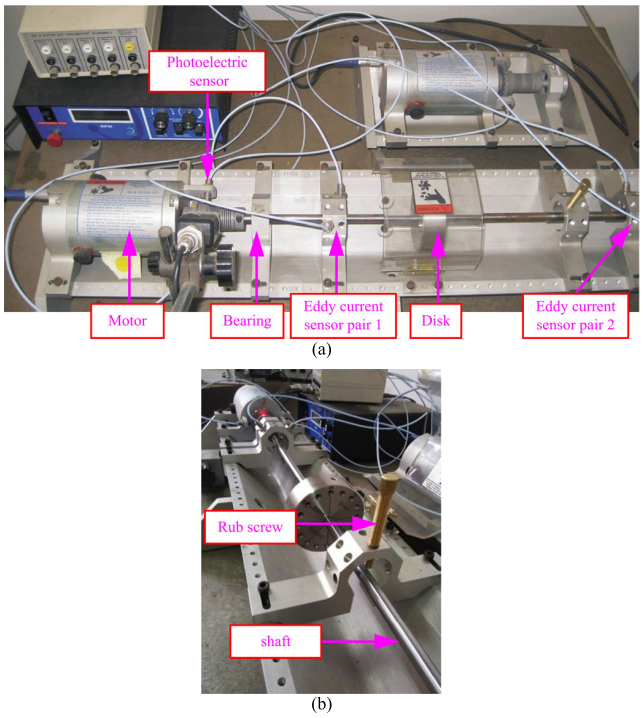

FIGURE 6. (a) The rotor experiment rig; (b) the rubbing device.

balancing disk, is attached to the motor through a connector. Two bearings are distributed at both ends of the shaft to provide sufficient support. In the experiment, a photoelectric sensor was installed near the keyway to obtain the key phase signal, and two pairs of eddy current sensors were arranged on both sides of the balance plate to measure the horizontal and vertical vibration signals of the shaft. Fig. 6(b) illustrates the rubbing device, in which the tightening degree of the rub screw can be regulated to control the force of rubbing. The experiment was conducted under the rotating speed of 3300 rpm, and the vibration data were recorded at a sampling frequency of 5120 Hz.

The vibration signals measured by the eddy current sensor pair 1 are adopted as the research objects. Figs. 7 and 8 show the waveforms of the horizontal and vertical vibration signals and their frequency spectrums. Among these two frequency spectrums, it is evident that only the 1X frequency component is outstanding, while the other harmonics of the fundamental frequency are too feeble to detect. The fault pattern cannot be determined based on the fault information extracted from a single channel. The axis orbit, synthesized by using these two signals, is shown in Fig. 9. There are some distinct cusps on the axis orbit, which reflect a fault feature of rubbing. However, it is vital to detect the substantial frequency components to further identify the fault type.

Next, a complex signal is constructed by using the horizontal and vertical vibration signals, and it is subjected to CSSD. Figs. 10(a) and (b) show the decomposed sequences of the positive and the negative frequency components. Based on the stopping criterion of decomposition, shown in Equation (4), four decomposed components are obtained. The decomposed

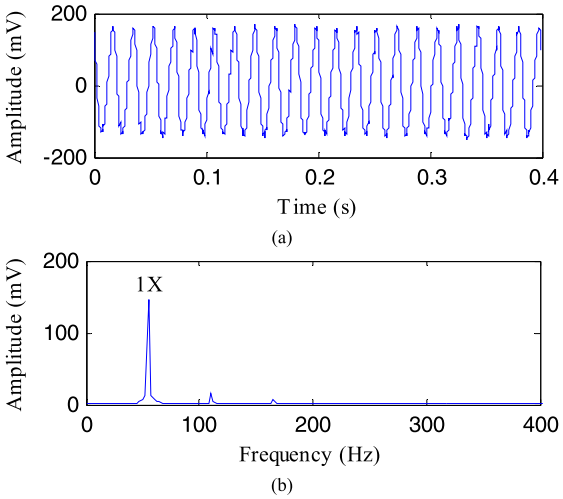

FIGURE 7. (a) The vibration signal in the horizontal direction and (b) its frequency spectrum.

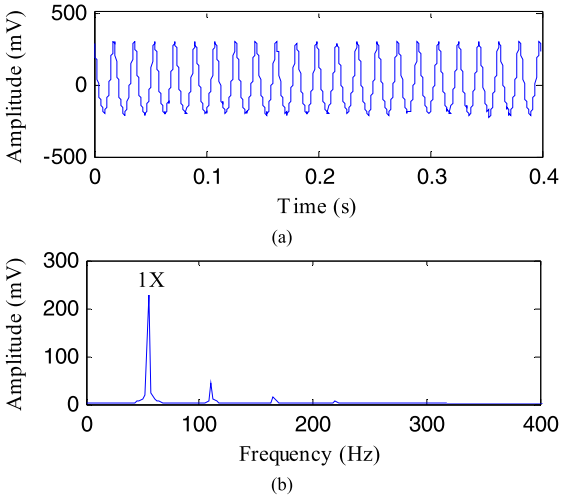

FIGURE 8. (a) The vibration signal in the vertical direction and (b) its frequency spectrum.

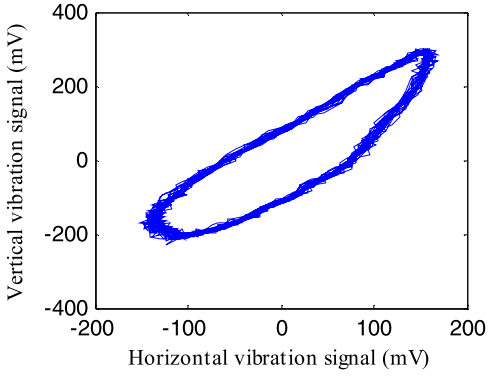

FIGURE 9. The axis orbit.

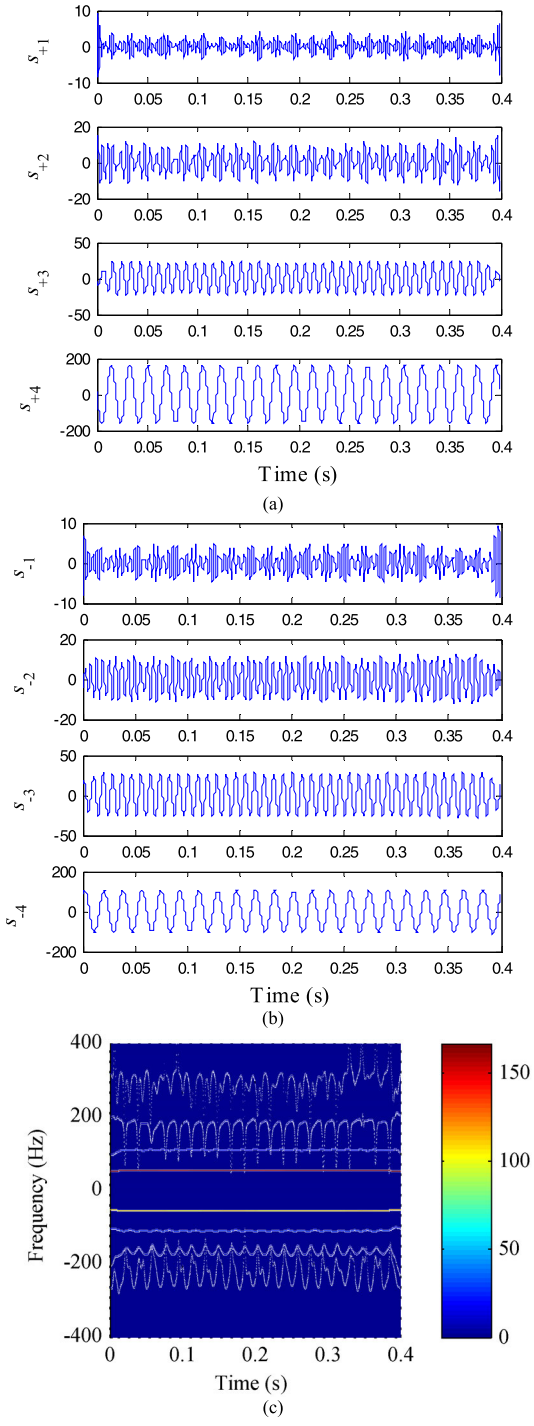

FIGURE 10. (a) The decomposed sequences of CSSD for the positive frequency component; (b) the decomposed sequences of CSSD for the negative frequency component and (c) the CSSD-HTFS.

sequences are composed of the impact-component and harmonic-component signals, which reveals the fault features of the rubbing. Fig. 10(c) illustrates the CSSD-HTFS, reflecting the positive and negative harmonics of the fundamental frequency. Moreover, the inter-wave demodulation characteristic can be visible in some of the frequency components of the CSSD-HTFS, which further demonstrates the fault signatures of the rubbing.

The analysis results obtained by applying the CEMD algorithm to the two-channel vibration signals are introduced for comparison. From the CEMD decomposition results of the positive and negative frequencies, as separately shown in Figs. 11(a) and (b), it is derived that some

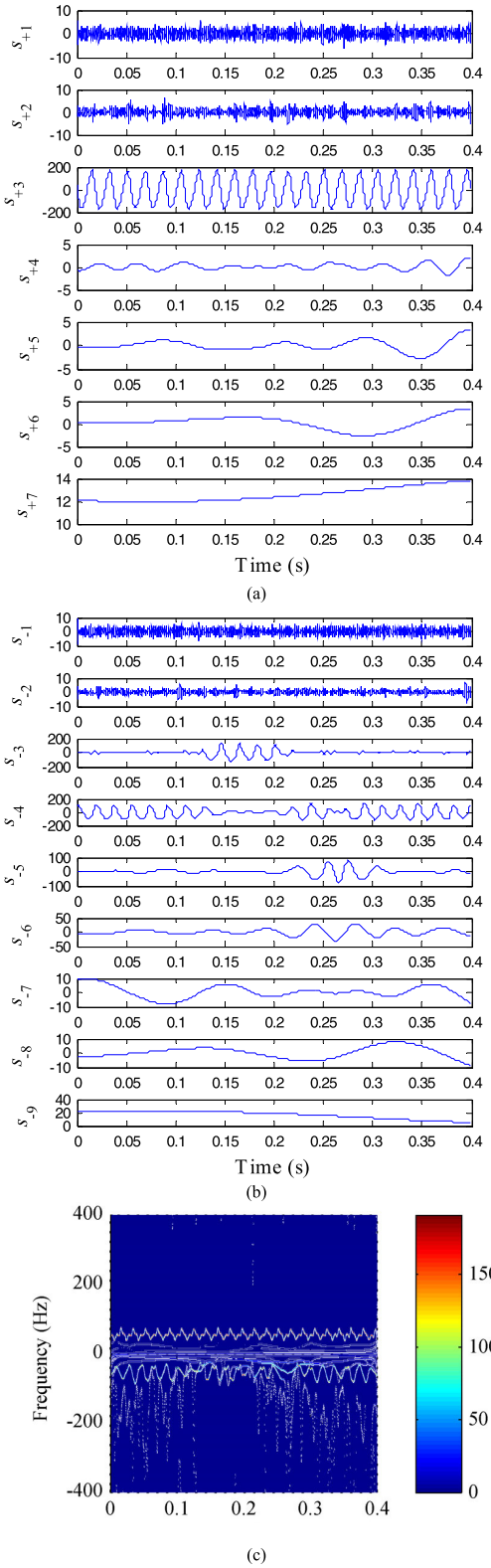

FIGURE 11. (a) The decomposed sequences of CEMD for the positive frequency component; (b) the decomposed sequences of CEMD for the negative frequency component and (c) the CEMD-HTFS.

components without physical meanings are generated by CEMD, illustrating the arise of the over-decomposition. Their CEMD Hilbert time-frequency spectrum (CEMD-HTFS), as

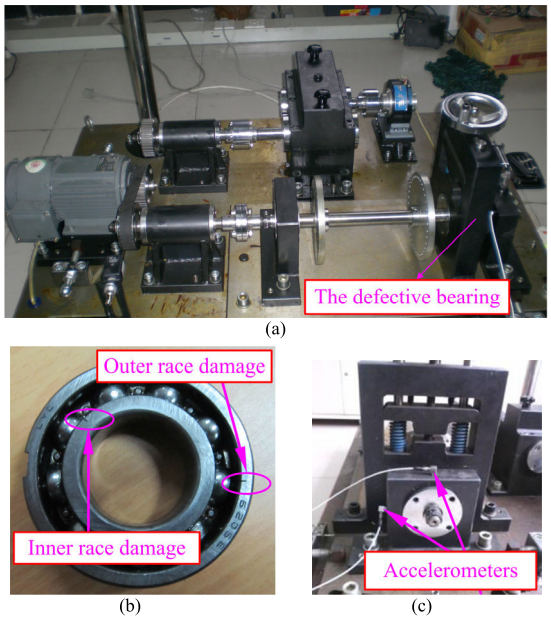

FIGURE 12. (a) The test bench; (b) the defective REB; (c) the layout of the sensors.

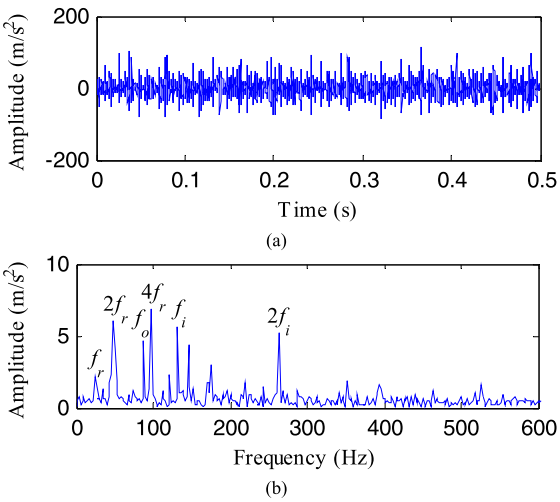

FIGURE 13. (a) The horizontal vibration signal and (b) its HES.

illustrated in Fig. 11(c), presents only the information related to the fundamental frequency, along with some unreasonable frequency components. The CSSD algorithm detects more sub-components with physical meanings and more sufficient signatures compared to the CEMD method.

B. ANALYSIS OF COMPOUND FAULT SIGNAL OF ROLLING ELEMENT BEARING

The vibration data of the compound fault of REB, obtained from the QPZZ-II rotating machinery test bench, is employed to further verify the capability of the proposed methodology. Fig. 12(a) shows the structure of the test bench, and the location of the faulty bearing has also been marked in this figure. The type of the experimental REB is LYC6205E. Fig. 12(b) depicts the defective REB, which shows both the

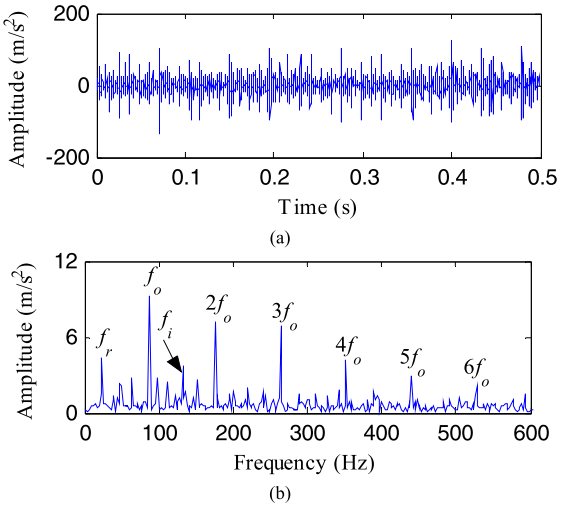

FIGURE 14. (a) The vertical vibration signal and (b) its HES.

TABLE 1. The geometric parameters of the defective REB.

Pitch diameter D/mm	Ball diameter d/mm	Number of balls Z	Contact angle γ/(°)
39	7.94	9	0

inner race and outer race damages. Fig. 12(c) represents the layout of the sensors. As depicted, two PCB accelerometers were placed on the horizontal-direction and vertical-direction of the bearing block, respectively. The position of the fault relative to the load zone of the bearing may affect the vibration response of the rotor-bearing system. Hence, two compound fault experiments were carried out with outer race fault located at 6 o'clock (i.e., the bottom of the bearing housing) and at 12 o'clock (i.e., the top of the bearing housing), respectively. Both experiments were conducted at motor speed $n = 1470$ rpm, i.e., at rotating frequency $f_r = 24.5$ Hz. The signal sampling rate is 12800 Hz. Based on the geometric parameters of the REB as illustrated in Table 1, the fault characteristic frequencies of the inner and outer race can be calculated as:

$$f_i = \frac{Z}{2}(1 + \frac{d}{D}\cos\gamma)\frac{n}{60} = 133 \text{ Hz}$$
$$f_o = \frac{Z}{2}(1 - \frac{d}{D}\cos\gamma)\frac{n}{60} = 88 \text{ Hz} \quad (19)$$

1) CASE 1: COMPOUND FAULT EXPERIMENT WITH OUTER RACE FAULT AT 6'CLOCK POSITION

First, the compound fault experiment of REB was conducted with outer race fault located at 6'clock position (directly in the load zone). Figs. 13 and 14 represent the waveforms and HESs of the vibration signals collected by the accelerometers in two directions. The two HESs exhibit considerable differences. The rotating frequency of the shaft and its harmonics are outstanding in the HES of the horizontal vibration signal,

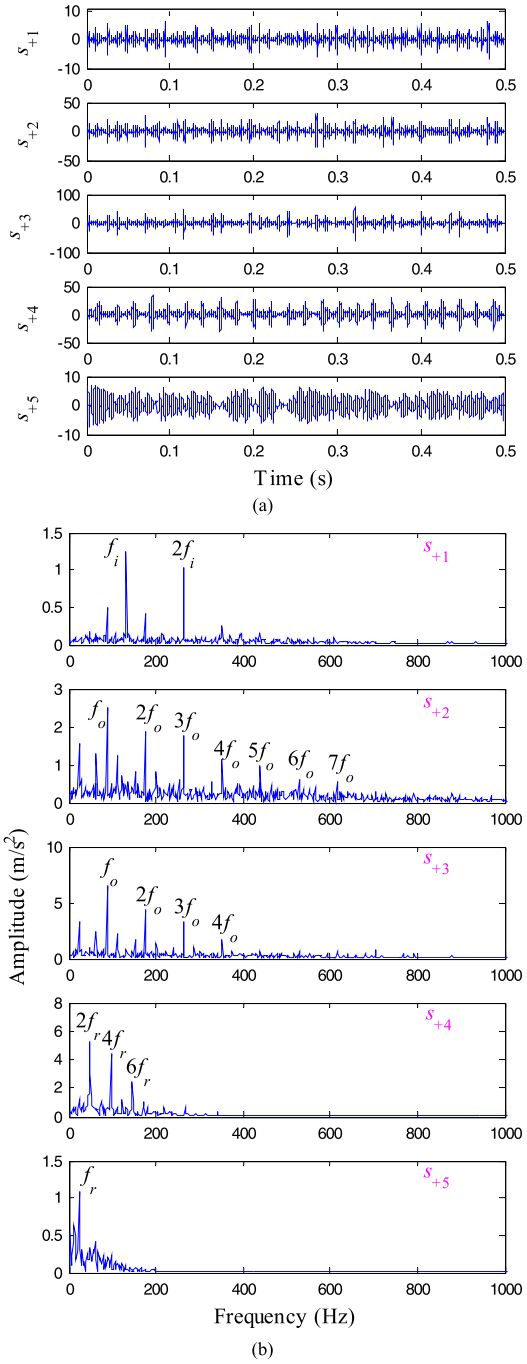

FIGURE 15. (a) The decomposed sequences of CSSD for the positive frequency component and (b) the CSSD-HES.

which increases the difficulty to detect the useful information. Despite the distinct spectral lines at the frequencies of f_i and $2f_i$ can be identified, the fault features of the outer race fault are not apparent. The HES of the vertical vibration signal is dominated by f_o and its harmonics, which denotes an apparent fault signature of the outer race fault. However, the spectral line associated with the inner race fault frequency is very feeble. It can be deduced that the vibration signals in different directions carry different fault information. It is

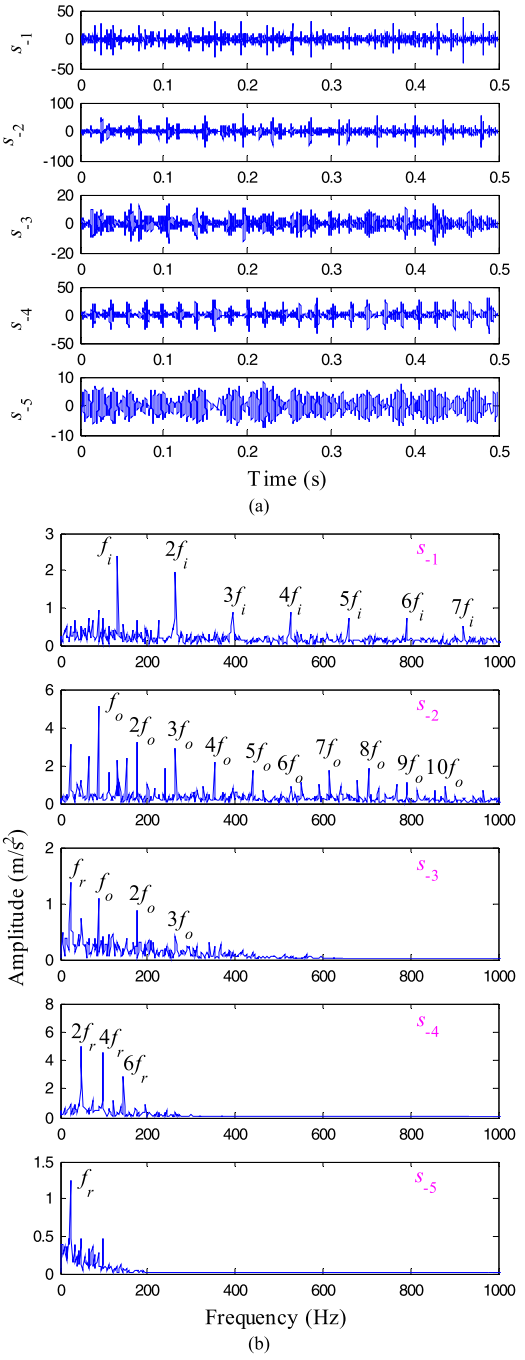

FIGURE 16. (a) The decomposed sequences of CSSD for the negative frequency component and (b) the CSSD-HES.

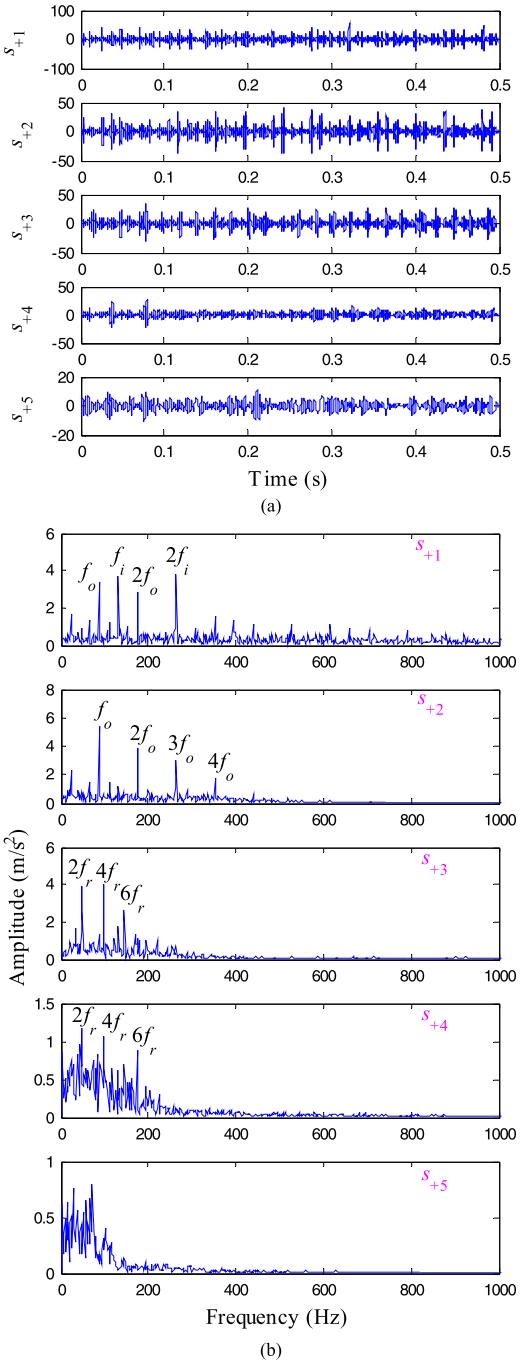

FIGURE 17. (a) The decomposed sequences of CEMD for the positive frequency component and (b) the corresponding HES.

very important to take effective measures to fuse the vibration information in different directions.

The proposed method is used to fuse the vibration information in different directions and separate the fault signatures from the interferences. A complex signal is synthesized according to step (2) in Section IV, and the complex signal is processed by CSSD. Since the fault features are mainly contained in the first few higher energy decomposed components, only the first five decomposed components are selected for analysis. Fig. 15(a) displays the decomposed components of the positive frequency component. Fig. 15(b) represents the CSSD-HES of theses decomposed components. Fig. 16 illustrates the analysis results of the negative frequency component. From Fig. 15(b) and Fig. 16(b), it is evident that the characteristic information corresponding to the inner race fault, outer race fault and the inherent vibration of the shaft is successfully isolated. Hence, we can obtain sufficient evidence to determine the compound fault pattern of the REB.

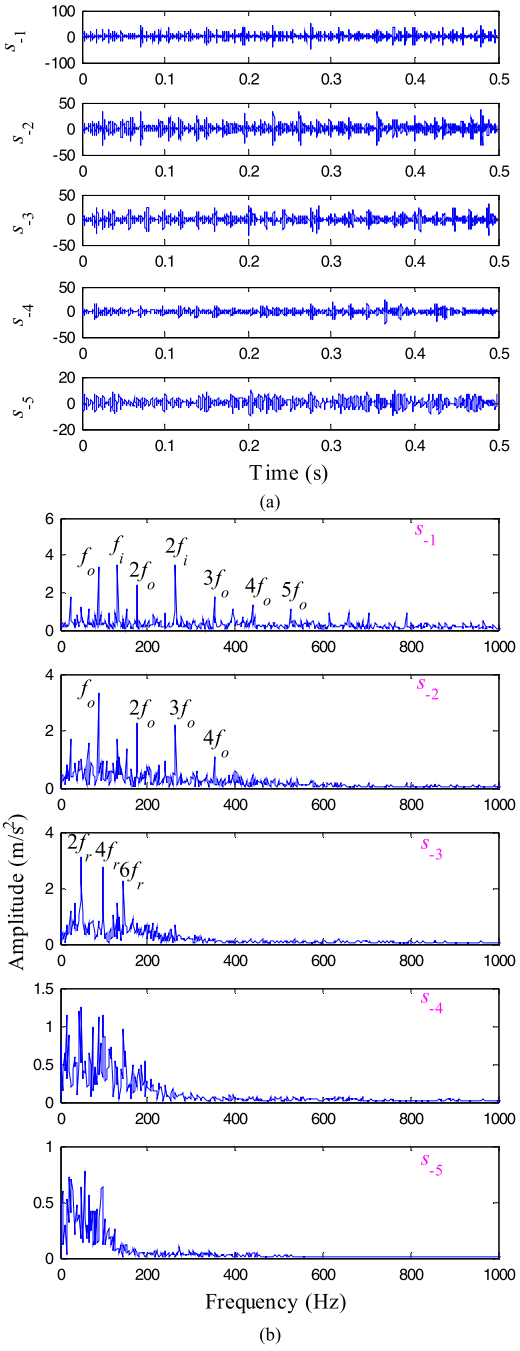

FIGURE 18. (a) The decomposed sequences of CEMD for the negative frequency component and (b) the corresponding HES.

The fault signal is also processed by the CEMD approach to make a comparison with the CSSD method. Fig. 17(a) and Fig. 18(a) show the decomposed components, which are yielded by conducting EMD on the positive and negative frequency components, respectively. Fig. 17(b) and Fig. 18(b) represent the HESs of these decomposed series. Note that, only the first five decomposed series are chosen for analysis. Some extra decomposed series without physical meanings are also generated after the

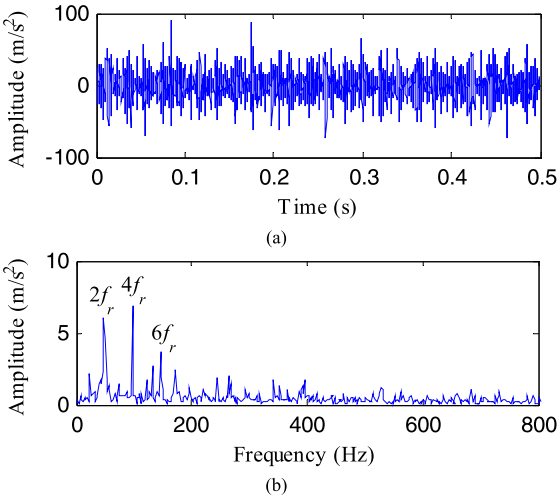

FIGURE 19. (a) The horizontal vibration signal and (b) its HES.

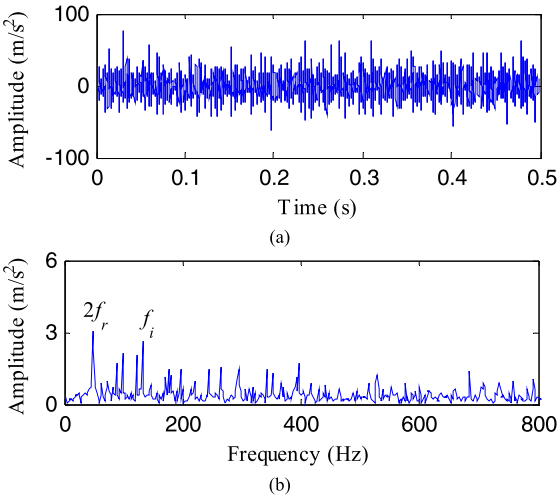

FIGURE 20. (a) The vertical vibration signal and (b) its HES.

CEMD decomposition. The fault features related to the inner and outer race fault can be located from the HES of the decomposed components s_{+1} and s_{-1}. However, the fault features of the two faults are mixed together, reflecting the mode mixing of CEMD. It can be inferred that the decomposition ability of the CSSD algorithm is stronger compared to the CEMD method.

2) CASE 2: COMPOUND FAULT EXPERIMENT WITH OUTER RACE FAULT AT 12'CLOCK POSITION

The vibration data of the compound fault experiment conducted with outer race fault located at 12'clock position is employed for analysis. Figs. 19 and 20 show the waveforms and HESs of the vibration signals collected in two directions. The dominant frequencies of the HES of the vibration signal in the horizontal direction are mainly composed of the harmonics of f_r, while the fault frequencies are invisible. Two obvious spectral lines associated with the frequencies

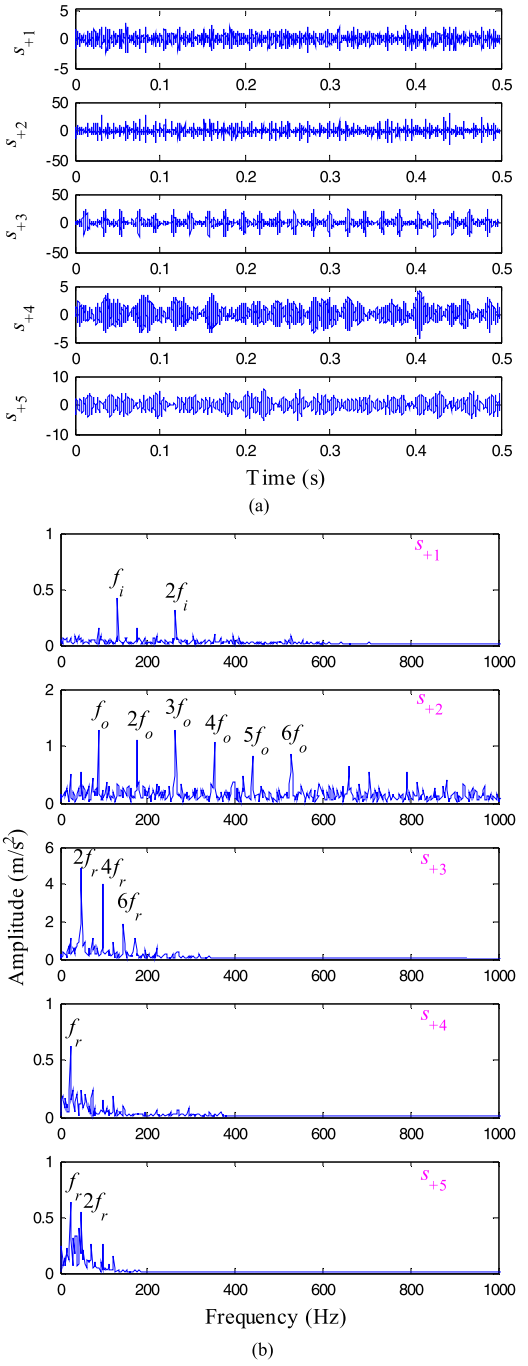

FIGURE 21. (a) The decomposed sequences of CSSD for the positive frequency component and (b) the CSSD-HES.

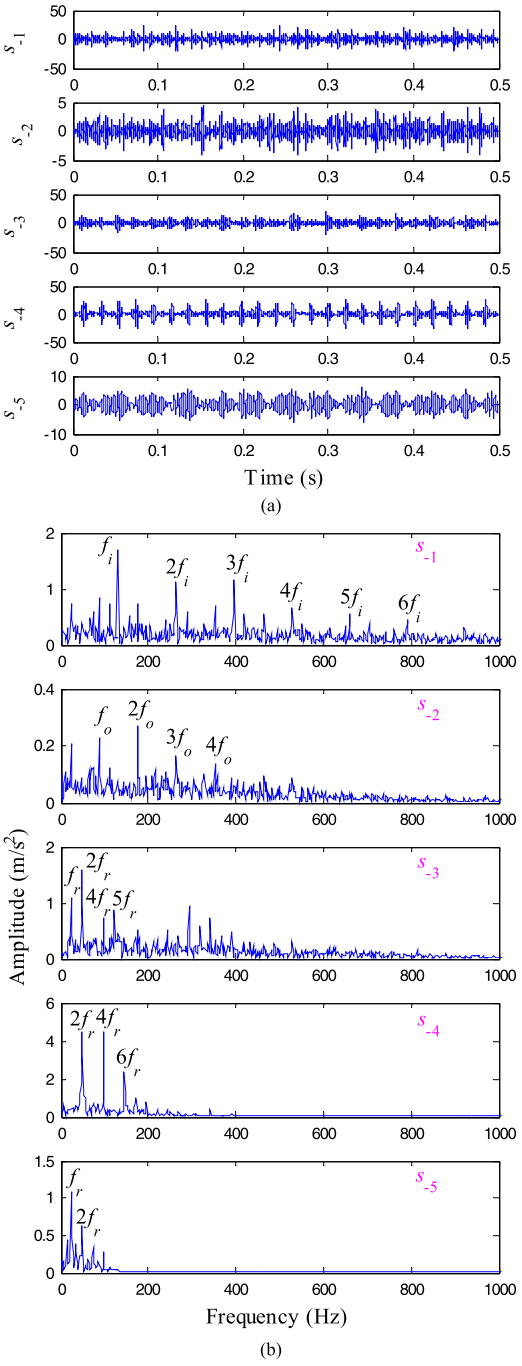

FIGURE 22. (a) The decomposed sequences of CSSD for the negative frequency component and (b) the CSSD-HES.

of $2f_r$ and f_i can be observed in the HES of the vertical vibration signal. However, the fault features corresponding to the outer race fault cannot be easily recognized. When the position of the outer race fault changes from 6 o'clock to 12 o'clock, the load on the outer race fault point decreases. Therefore, the fault features of the outer race become inconspicuous.

The proposed method is employed to extract the fault features of the compound fault. Fig. 21(a) and Fig. 22(a) display the decomposed components of the CSSD algorithm. Fig. 21(b) and Fig. 22(b) exhibit the CSSD-HES of the decomposed components as shown in Fig. 21(a) and Fig. 22(a), respectively. It can be found that the fault features of the inner race fault and the outer race fault are separated. The analysis results of Case 1 and Case 2 demonstrate that the proposed method can get rid of the influence of the placement of the fault relative to the load zone.

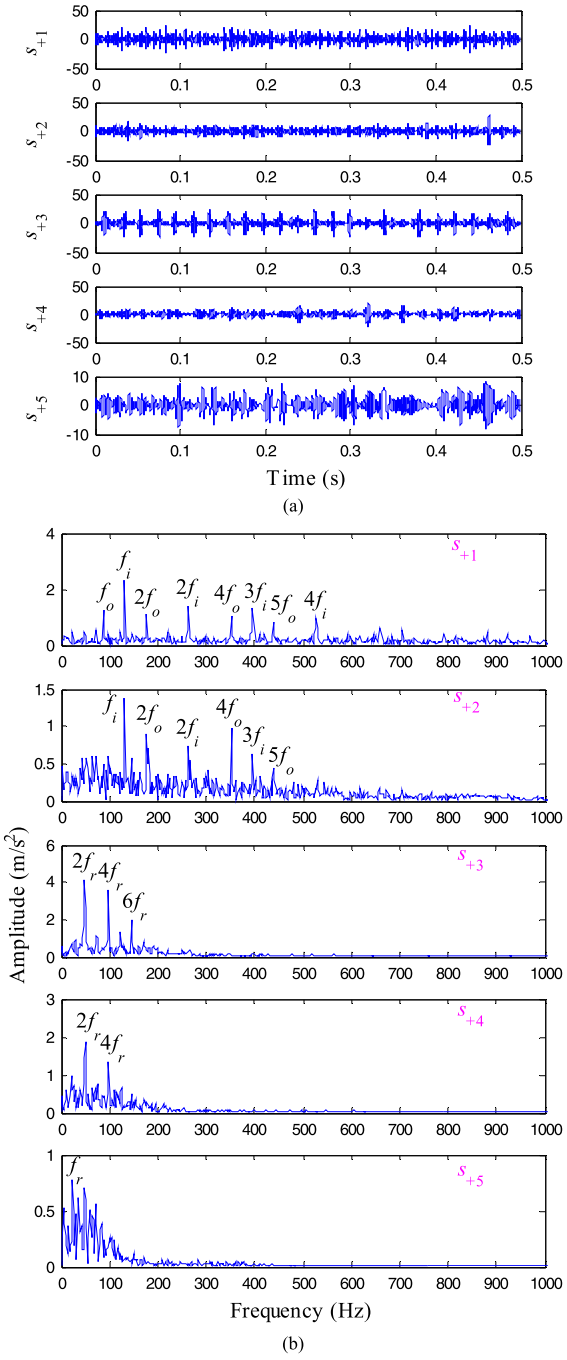

FIGURE 23. (a) The decomposed sequences of CEMD for the positive frequency component and (b) the corresponding HES.

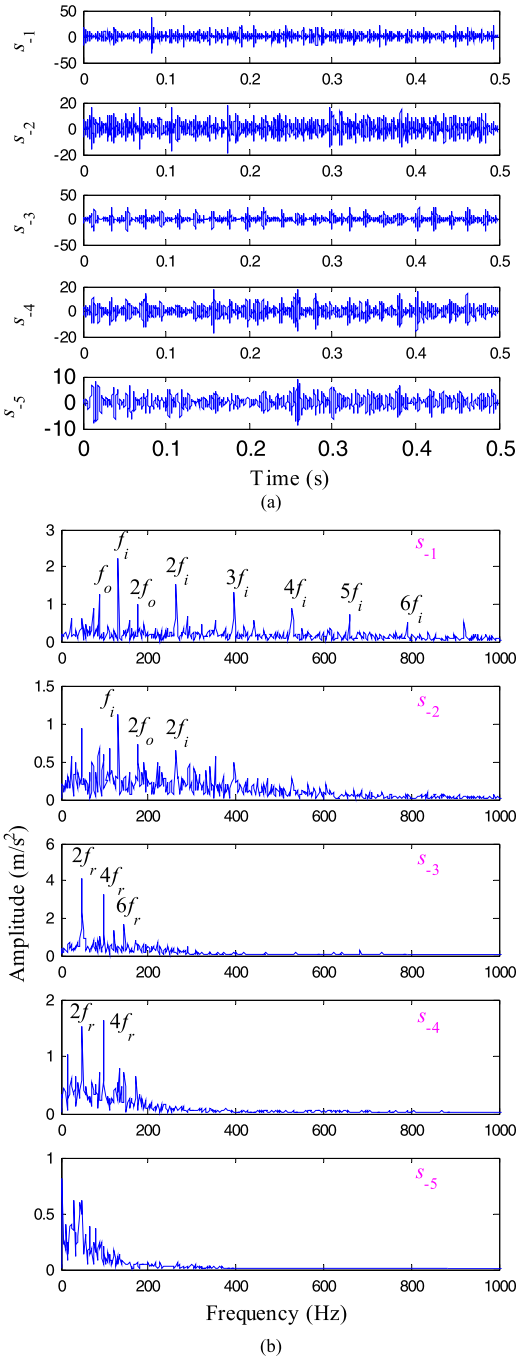

FIGURE 24. (a) The decomposed sequences of CEMD for the negative frequency component and (b) the corresponding HES.

Figs. 23 and 24 show the analysis results obtained by applying CEMD to the compound fault signal. It can be found that the fault features of the inner race fault and the outer race fault extracted by the CEMD method are mixed, revealing the "mode mixing" problem of CEMD. The CSSD algorithm is more effective in separating the fault features compared to the CEMD algorithm.

VI. CONCLUSION

This paper presents a CSSD algorithm, which aims to extend the real-valued SSD to the complex-valued domain. It is implemented by separately applying SSD to the positive and negative frequency components of a complex-valued signal. The Gaussian noise test indicates that the CSSD method can perform as a filter bank. Combining the advantages of CSSD and HT, two fault feature detection approaches, termed CSSD-HTFS and CSSD-HES, are developed. A novel

fault diagnosis framework for rotating machinery is proposed based on the developed algorithms. Experimental applications demonstrate that the proposed CSSD algorithm can realize the homologous information fusion and extract sufficient fault signatures. Moreover, the proposed CSSD approach performs better in overcoming the problem of mode mixing compared to the CEMD technique.

Note that the current work focuses on the framework for processing the vibration signals of only two channels by using CSSD. In the future, the application of the proposed method for more channels will be explored. Finally, this research aims to inspire more research into the advantages of complex signal analysis.

REFERENCES

[1] Y. Li, X. Wang, Z. Liu, X. Liang, and S. Si, "The entropy algorithm and its variants in the fault diagnosis of rotating machinery: A review," *IEEE Access*, vol. 6, pp. 66723–66741, 2018.
[2] R. Liu, B. Yang, E. Zio, and X. Chen, "Artificial intelligence for fault diagnosis of rotating machinery: A review," *Mech. Syst. Signal Process.*, vol. 108, pp. 33–47, Aug. 2018.
[3] A. Glowacz, "Fault diagnosis of single-phase induction motor based on acoustic signals," *Mech. Syst. Signal Process.*, vol. 117, pp. 65–80, Feb. 2019.
[4] Z. Wang, L. Zheng, W. Du, W. Cai, J. Zhou, J. Wang, X. Han, and G. He, "A novel method for intelligent fault diagnosis of bearing based on capsule neural network," *Complexity*, vol. 2019, Jun. 2019, Art. no. 6943234.
[5] D. Wang, "Spectral L2/L1 norm: A new perspective for spectral kurtosis for characterizing non-stationary signals," *Mech. Syst. Signal Process.*, vol. 104, pp. 290–293, May 2018.
[6] Z. Wang, W. Du, J. Wang, J. Zhou, X. Han, Z. Zhang, and L. Huang, "Research and application of improved adaptive MOMEDA fault diagnosis method," *Measurement*, vol. 140, pp. 63–75, Jul. 2019.
[7] Z. Feng, D. Zhang, and M. J. Zuo, "Adaptive mode decomposition methods and their applications in signal analysis for machinery fault diagnosis: A review with examples," *IEEE Access*, vol. 5, pp. 24301–24331, 2017.
[8] H. Y. Pan, Y. Yang, X. Li, J. D. Zheng, and J. S. Cheng, "Symplectic geometry mode decomposition and its application to rotating machinery compound fault diagnosis," *Mech. Syst. Signal Process.*, vol. 114, pp. 189–211, Jan. 2019.
[9] N. E. Huang, Z. Shen, S. R. Long, M. C. Wu, H. H. Shih, Q. Zheng, N.-C. Yen, C. C. Tung, and H. H. Liu, "The empirical mode decomposition and the Hilbert spectrum for nonlinear and non-stationary time series analysis," *Proc. Roy. Soc. London A, Math. Phys. Eng. Sci.*, vol. 454, no. 1971, pp. 903–995, Mar. 1998.
[10] Z. Wang, J. Wang, W. Cai, J. Zhou, W. Du, J. Wang, G. He, and H. He, "Application of an improved ensemble local mean decomposition method for gearbox composite fault diagnosis," *Complexity*, vol. 2019, May 2019, Art. no. 1564243.
[11] J. Zheng, J. Cheng, and Y. Yang, "A rolling bearing fault diagnosis approach based on LCD and fuzzy entropy," *Mech. Mach. Theory*, vol. 70, pp. 441–453, Dec. 2013.
[12] J. Zhang, J. Zhang, M. Zhong, J. Zhong, J. Zheng, and L. Yao, "Detection for incipient damages of wind turbine rolling bearing based on VMD-AMCKD method," *IEEE Access*, vol. 7, pp. 67944–67959, 2019.
[13] Z. Wang, G. He, W. Du, J. Zhou, X. Han, J. Wang, H. He, X. Guo, J. Wang, and Y. Kou, "Application of parameter optimized variational mode decomposition method in fault diagnosis of gearbox," *IEEE Access*, vol. 7, pp. 44871–44882, Apr. 2019.
[14] J. Cheng, Y. Peng, Y. Yang, and Z. Wu, "Adaptive sparsest narrow-band decomposition method and its applications to rolling element bearing fault diagnosis," *Mech. Syst. Signal Process.*, vol. 85, pp. 947–962, Feb. 2017.
[15] Y. Miao, M. Zhao, V. Makis, and J. Lin, "Optimal swarm decomposition with whale optimization algorithm for weak feature extraction from multicomponent modulation signal," *Mech. Syst. Signal Process.*, vol. 122, pp. 673–691, May 2019.
[16] X. Xu, M. Zhao, and J. Lin, "Detecting weak position fluctuations from encoder signal using singular spectrum analysis," *ISA Trans.*, vol. 71, pp. 440–447, Nov. 2017.
[17] P. Bonizzi, J. M. H. Karel, O. Meste, and R. L. M. Peeters, "Singular spectrum decomposition: A new method for time series decomposition," *Adv. Adapt. Data Anal.*, vol. 6, no. 4, 2014, Art. no. 1450011.
[18] B. Pang, G. Tang, and T. Tian, "Enhanced singular spectrum decomposition and its application to rolling bearing fault diagnosis," *IEEE Access*, vol. 7, pp. 87769–87782, 2019.
[19] J. Wang, X. Han, Z. Wang, W. Du, J. Zhou, J. Zhang, H. He, and X. Guo, "Modified singular spectrum decomposition and its application to composite fault diagnosis of gearboxes," *Sensors*, vol. 19, no. 1, p. 62, 2019.
[20] X. Chen, L. Peng, G. Cheng, and C. Luo, "Research on degradation state recognition of planetary gear based on multiscale information dimension of SSD and CNN," *Complexity*, vol. 2019, Mar. 2019, Art. no. 8716979.
[21] C. L. Keppenne and U. Lall, "Complex singular spectrum analysis and multivariate adaptive regression splines applied to forecasting the southern oscillation," *Exp. Long Lead Forecast Bull.*, vol. 5, pp. 54–56, Mar. 1996.
[22] V. Georgescu and S.-M. Delureanu, "Fuzzy-valued and complex-valued time series analysis using multivariate and complex extensions to singular spectrum analysis," in *Proc. IEEE Int. Conf. Fuzzy Syst. (FUZZ-IEEE)*, Aug. 2015, pp. 1–8.
[23] G. Rilling, P. Flandrin, P. Gonçalves, and J. M. Lilly, "Bivariate empirical mode decomposition," *IEEE Signal Process. Lett.*, vol. 14, no. 12, pp. 936–939, Dec. 2007.
[24] W. Yang, R. Court, P. J. Tavner, and C. J. Crabtreeb, "Bivariate empirical mode decomposition and its contribution to wind turbine condition monitoring," *J. Sound Vib.*, vol. 330, no. 15, pp. 3766–3782, 2011.
[25] C. Park, D. Looney, M. M. Van Hulle, and D. P. Mandic, "The complex local mean decomposition," *Neurocomputing*, vol. 74, no. 6, pp. 867–875, 2011.
[26] T. Tanaka and D. P. Mandic, "Complex empirical mode decomposition," *IEEE Signal Process. Lett.*, vol. 14, no. 2, pp. 101–104, Feb. 2007.
[27] Y. Wang, F. Liu, Z. Jiang, S. He, and Q. Mo, "Complex variational mode decomposition for signal processing applications," *Mech. Syst. Signal Process.*, vol. 86, pp. 75–85, Mar. 2017.
[28] H. Yu, H. Li, Y. Li, and Y. Li, "A novel improved full vector spectrum algorithm and its application in multi-sensor data fusion for hydraulic pumps," *Measurement*, vol. 133, pp. 145–161, Feb. 2019.
[29] P. Flandrin, G. Rilling, and P. Goncalves, "Empirical mode decomposition as a filter bank," *IEEE Signal Process. Lett.*, vol. 11, no. 2, pp. 112–114, Feb. 2004.

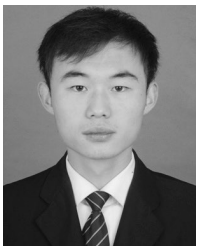

BIN PANG received the M.S. degree in mechanical engineering from North China Electric Power University, China, in 2015, where he is currently pursuing the Ph.D. degree in mechanical engineering. His research interests include signal processing and rotating machinery fault diagnosis. His awards and honors include the National Scholarship and the Excellent Master's Thesis of Hebei Province, China.

GUIJI TANG received the B.S., M.S., and Ph.D. degrees from North China Electric Power University, China, in 1983, 1991, and 1999, respectively, where he is currently a Professor with the Department of Mechanical Engineering. His research interests include state monitoring and fault diagnosis of rotating machinery, and dynamic characteristics analysis of power machinery structure.

TIAN TIAN received the B.S. and M.S. degrees in mechanical engineering from North China Electric Power University, China, in 2016 and 2019, respectively, where she is currently pursuing the Ph.D. degree in mechanical engineering. Her research interests include signal processing and rotating machinery fault diagnosis.